Supplementary information: Towards a phenomenological description of the airborne release of hazardous particles during thermal degradation of contaminated polycarbonate surfaces.

F.-X. Ouf[a], T. Gelain[a], M. Patry[a] and F. Salm[a]
[a]Institut de Radioprotection et de Sûreté Nucléaire (IRSN), PSN-RES, SCA, Gif-Sur-Yvette, 91192, France.

Corresponding author: francois-xavier.ouf@irsn.fr

Supplementary information SI1: Computation of number of particles mono-layer of the deposit

In parallel with the determination of the mass of particles deposited on the sample, it is also necessary to estimate, based on the surface concentration and properties of the particles, the number of mono-layer characterizing the deposit on the surface of the polymer. With spherical particles, the density ρ_p of a particle of equivalent volume diameter D_{ev} is determined by the following formula:

$$m_P = \rho_P V_P \text{ where } V_P = \frac{1}{6}\pi D_{ev}^3 .$$

So the mass of a particle m_P is:

$$m_P = \frac{1}{6}\pi \rho_P D_{ev}^3 .$$

On a polycarbonate surface S, the surface contamination C_M (i.e. the mass of particles per unit area) associated with a number N_p of particles of mass m_p is defined by:

$$C_M = \frac{N_P m_P}{S} = \frac{N_P \pi \rho_P D_{ev}^3}{6S}.$$

The concentration in terms of the number of particles per unit area C_N can be defined by:

$$C_N = \frac{C_M}{m_P}.$$

The projected area S_p per particle (in the case of a 2D stack) is given by:

$$S_P = \pi \frac{D_{ev}^2}{4}.$$

The number of mono-layer N_{mono} of particles therefore takes the form:

$$N_{mono} = \frac{S_P C_N}{0.91}.$$

0.91 is the ideal compactness (ratio of area occupied by spheres to total area) of a 2D stack of spherical particles. Figure SI1-1 presents the evolution of N_{mono} for PuO_2 particles as a function of deposited mass per surface area for several equivalent volume diameters. For contamination levels considered in the present study, aiming to mimic industrial situation, i.e. up to 1 mg/cm², deposit is characterized by less than one mono-layer.

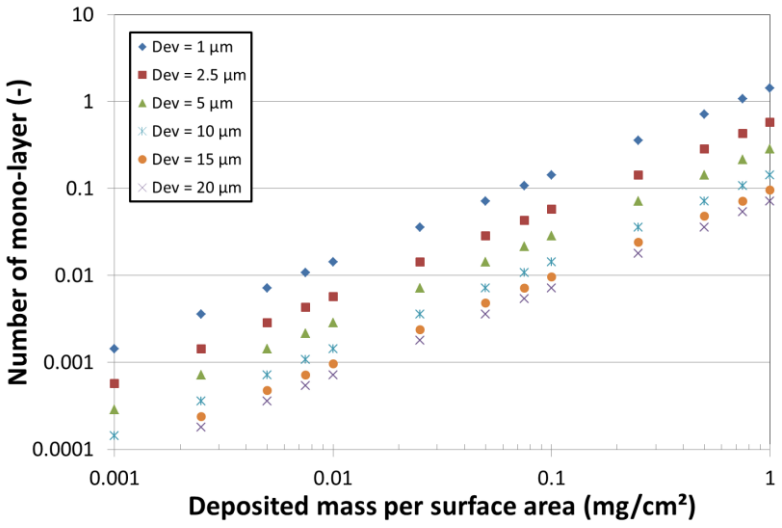

Figure SI1-1: evolution of N_{mono} as a function of deposited mass per surface area C_M of PuO_2 particles

Supplementary information SI2: experimental measurement and CFD computation of particle losses within the test bench

To check the representativeness of the aerosol samples taken in the test bench with the proposed powders, it is necessary to determine particle losses in the whole transport and sampling line. For convenience, we will use the term penetrating fraction $F_{p(\%)}$, which represents the percentage of particles transported without loss through the whole transport and sampling installation. Two approaches to quantify this fraction were considered. The first one is based on experiments and the second one is based on CFD simulations using the ANSYS™ CFX software. One must notice that application of present experimental and CFD values of $F_{p(\%)}$ to calculation of ARF in ARTEMIS experiments assume size distribution of particles released from PC surface similar to size distributions of powders used as deposit.

Experimental approach

Experimentally, particles were injected into the test bench installation homogeneously using a PALAS™ RBG 1000 rotating brush generator. Once the particles have been generated, two stages were considered to measure the penetration factor:

- the first is to check the stability of particle generation and to determine the reference mass rate of particles injected in the test bench. To do this, a filter cartridge is installed and connected to the RBG 1000 and to the test bench (as shown in the top part of figure SI2-1). The particles are drawn by a flow of air controlled by a flow meter and adjusted with a valve. A glove box filter ensures the air discharged is 'clean'. During this experiment, three readings are taken of the mass deposited on a HEPA filter during a time t. If the mass is stable (+/- 10%), the next stage can begin;
- once the particle generation is known to be stable, the particles are directly injected via a tube into the test bench installation during the same time t. At the end of the experiment, the mass sampled on the filter $m_{sampled}$ (in the sampling area) is determined by successive weighings. It is then possible to determine the penetrating fraction of the particles. The bottom part of figure SI2-1 shows the rig used in this second step.

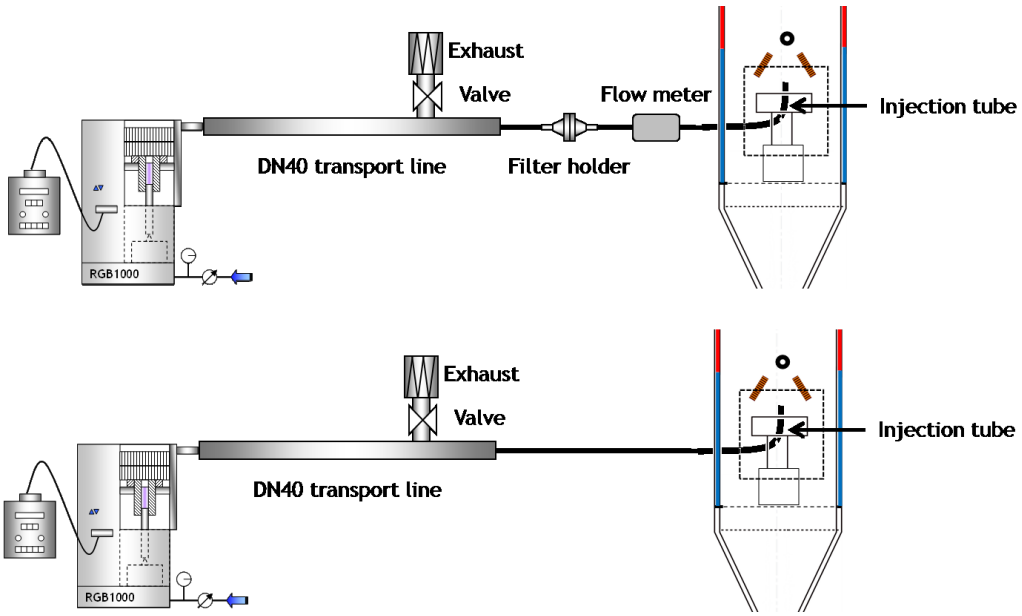

Figure SI2-1: experimental setup for characterizing penetration fraction within the combustion test bench. Upper part corresponds to measurement of injection mass rate of particles and lower part corresponds to direct injection within the test bench

For these experiments, the generation volume flow rate is set to 10 l/min. It is checked at each stage of the particle tracing in the test bench. The large piston of RBG-1000 has been set to rise at a speed of 20 mm/h. The temperature of the walls of the test has been set to 150°C and the radiant panel was not used.

The formula below is for the calculation of the penetrating fraction in the test bench taking account of losses.

$$F_{p(\%)}=\frac{m_{sampled,\ corrected}}{P_{p(\%)}.D_{\theta}.t}.$$

The corrected sampled mass $m_{sampled,corrected}$ taking account of powder losses in the injection tube (see figure SI2-1) implemented in the test bench ($m_{deposited\ injection}$) can be determined according to following relation:

$$m_{sampled,\ corrected}= m_{sampled} +P_{p(\%)}.m_{deposited,injection}$$

where:

- $F_p(\%)$: penetrating fraction of particles (%),
- $P_{p(\%)}$: percentage sampled on the membrane (here $P_{p(\%)}$ = 1.71%),
- D_{θ}: particle generation mass flow rate (mg/s),
- $m_{deposited,\ injection}$: mass of particles deposited in the injection tube after generation (g)[1],
- t: sampling time of 300 seconds.

The particle tracing experiment was conducted on 11 different powders. For all these species, we carried out 4 stability tests (stage 1 of the protocol) and 3 particle tracing tests (stage 2). The results are averaged and the uncertainties calculated.

CFD approach

In parallel to the experimental development, modelling of the installation and simulations of the experiment were also carried out. The purpose of this modelling is to compare the experimental and numerical penetrating fractions.

Modelling of the test bench was done using the ANSYS CFX general-purpose CFD software. This software was enriched with aerosol transport and deposition models and a DQMOM (Direct Quadrature Method of Moments) population model to transport the moments characterising a polydisperse size distribution, which has been assumed, in the present case, as lognormal (Gelain et al., 2018).

The simulations are done in several different stages: geometry creation, mesh generation and data set production (pre-processing), launch of the simulations and post-processing. These stages are presented below.

- *Geometry*

The geometry of the test bench installation was created using the ANSYS Design Modeler software and is shown in figure SI2-2 (left part).

- *Mesh*

The mesh of the geometry of the test bench was created using the ANSYS Meshing software and consists of 2.8 million tetrahedral elements. This mesh is refined in the areas of interest such as the injection area and the sampling area (middle part of figure SI2-2).

[1] This mass was determined after generation by weighing the injection tube, the geometry of which is not ideal for all powders used due to the constraints of the combustion test bench.

- *Data set*

Simulations require the production of a data set from the mesh generated earlier. This data set is used to define the input data as well as the boundary conditions of the computational domain representative of the experimental test bench. The numerical parameters of the computation, given in table SI2-1, are defined.

Table SI2-1: parameters considered for computations

Parameter type	Condition
Turbulence model	SST (Shear Stress Transport) k-ω model
Numerical scheme	High Resolution hybrid scheme
Convergence	Stationnary computation
	MAX residual = 10^{-5}
Time-scale	Physical time step = 0.5 s

The boundary conditions are shown in figure SI2-2 (right) and described in table SI2-2. Figure SI2-2 right also shows the monitoring points (yellow crosses), which are points in the domain used to monitor in real time the variables evolution and judge the convergence of the computation.

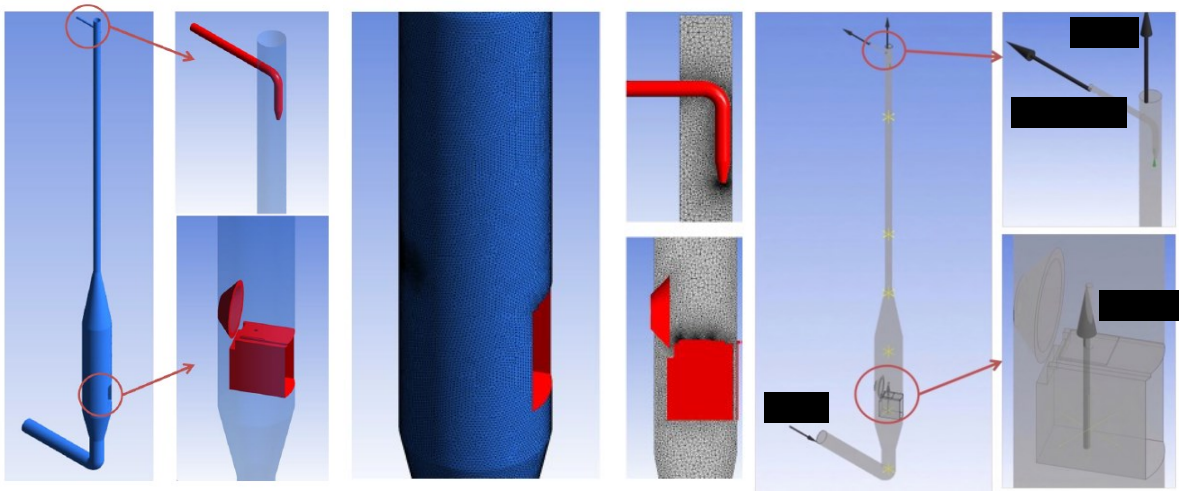

Figure SI2-2: geometry (left), mesh (middle) of the test bench as respectively created using the ANSYS Design Modeler and ANSYS Meshing softwares and illustration of boundary conditions (right)

Table SI2-2: boundary conditions considered for the computations

Boundary	Condition	Parameters
Inlet	"Inlet"	Velocity: U_{inlet} and Temperature: T_{inlet} Turbulent scales: $k = \frac{3}{2}(I\ U_{inlet})^2, \varepsilon = C_\mu \rho \frac{k^2}{\mu_t}$ where $\mu_t = 1000 I\mu$ (I = 3.7 %) and $\omega = \frac{\varepsilon}{k}$ Mass fraction of particles: $Y_p = 0$
Injection		Mass flow: Q_{inj} and Temperature: T_{inj} Mass fraction of particles: $Y_p = 1$
Outlet	"Outlet"	Relative pressure: $P_{outlet} = 0\ Pa$
Outlet_Prel		Mass flow: q_{prel}
Walls	"Wall"	No Slip Condition $U_{wall} = 0$ and "automatic" wall law Temperature: T_{wall}

The input data (see Table SI2-3) associated with the tests carried out are used to give the boundary conditions described in table SI2-1, as well as the data related to the particles.

Table SI2-3: input data considered for the computations

Data type	Value considered
Input flow rate Q_{inlet}	20 or 40 $m^3.h^{-1}$ (depending on the type of particles injected)
Injection flow rate Q_{inj}	10 $l.min^{-1}$
Sampling flow rate Q_{prel}	13.07 $Nl.min^{-1}$
Input temperature T_{inlet} and T_{inj}	20°C
Wall temperature T_{wall}	150°C
Aerodynamic diameter of the particles studied	See Table 7

Experimental and numerical results

The penetrating fractions obtained experimentally and numerically range from 3.2% to 105.1%, underlining the very significant influence of the aerodynamic diameter of the particles injected into the test bench (figure SI2-3). Plain black line represents results obtained for Al_2O_3 particles denoting geometric standard deviation of 2.2. Increasing the aerodynamic diameter for a single simulant causes a significant reduction in the penetrating fraction. However, the value 105.1% will not be taken into account as it is, since the test bench obviously cannot be used to produce tungsten carbide particles. A value like this should be weighted by its standard deviation, which for this sample is relatively large. We therefore consider a penetrating fraction of 100% for this simulant (WC). Note that the mean penetrating fraction and the error bars associated, shown in figure SI2-3 for the CFX computation results, were calculated at convergence and by considering a fixed number of time-steps (nearly 1000). Figure SI2-3 also shows the ratios of the total deposit associated with the transport line of the test bench and the sampling probe, which highlights the major contribution made by this sampling probe to the total fraction deposited for particles denoting MMAD larger than 10 µm.

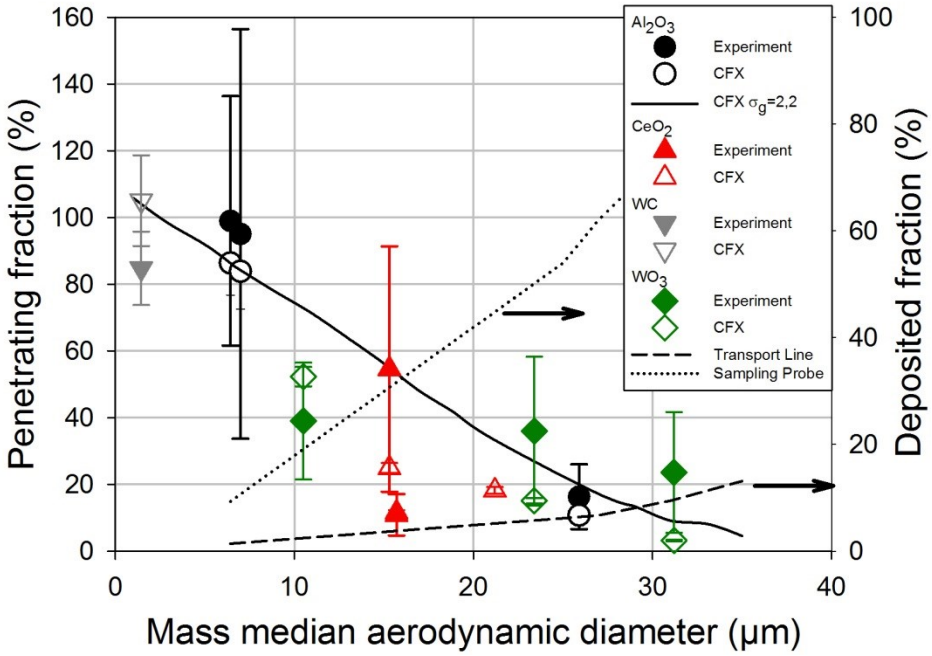

Figure SI2-3: influence of the mass median aerodynamic diameter on the penetrating fraction

Figure SI2-4 shows the comparison between the penetrating fraction obtained experimentally and numerically. An acceptable level of agreement between these two approaches could be noticed. The biggest differences are obtained for the samples «WO_3 D17», «CeO_2 US NANO D5» and «WO_3 D27», the structure of which in the first two cases is long, fine needles and in the third case are porous. For these morphologies, the assumption that particles are spherical, which is implicit in the aerosol deposition models used in CFX computation, undoubtedly reaches its limits.

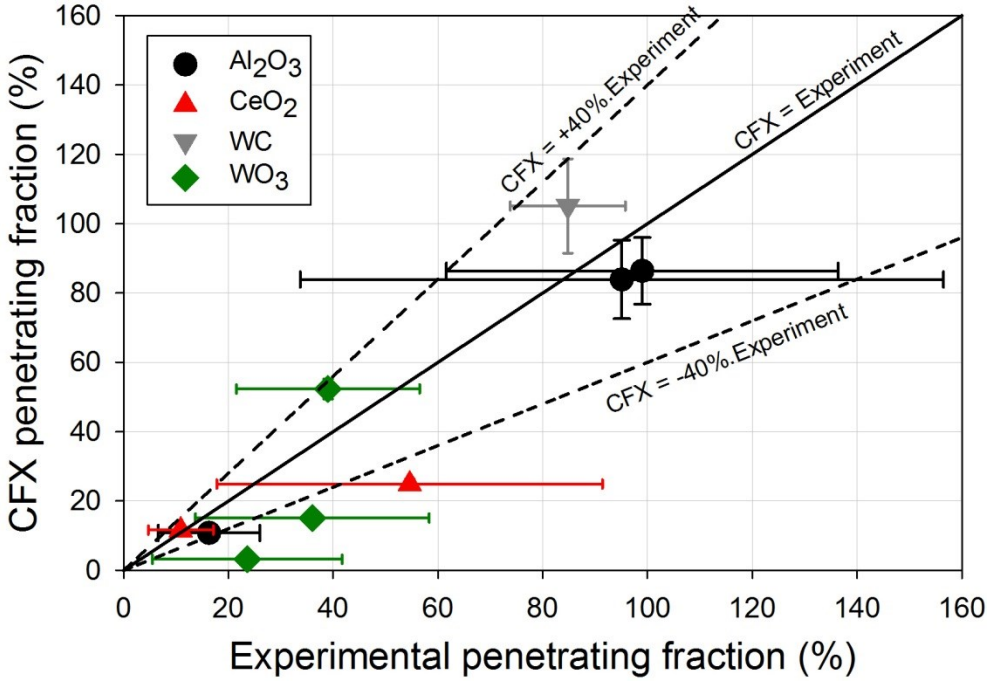

Figure SI2-4: parity diagram between experimental and numerical penetrating fractions

Supplementary information SI3: contact angle measurement protocol

The experimental protocol for measuring contact angle is as follows and properties of powders considered as particles deposit on the surface of glass sheet and in contact with PC granules and droplets are detailed in table SI3-1:

- Contamination of glass slides using the dispersion device.
- Mounting of contaminated glass slides and 6 PC granules in the DSA100 chamber (figure SI3-1).
- Melting of the PC granules at 200-210°C and stabilization for 180 min (figure SI3-1).
- Determination for each droplet of the contact angle on several image acquisitions (figure SI3-1).

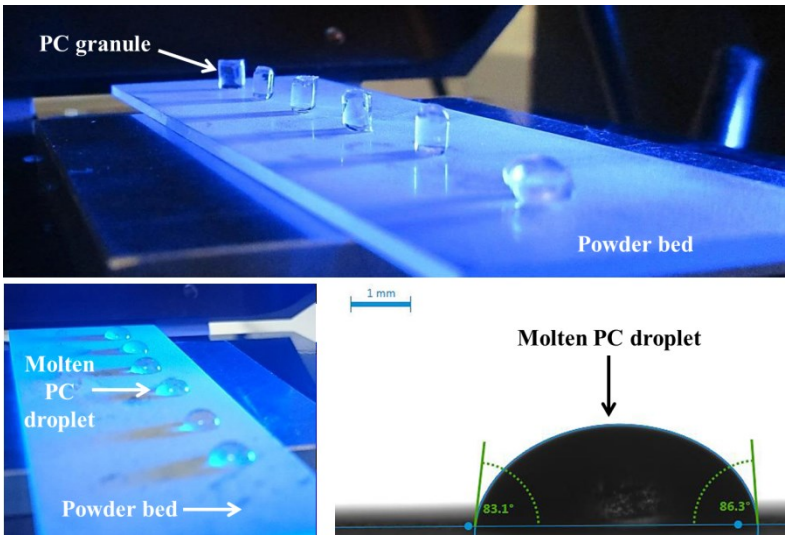

Figure SI3-1: experimental process for KRÜSS® DSA100 contact angle measurement

Table SI3-1: characteristics of the powders used to measure the contact angle

Particle characteristics						
Type of particles	Alumina oxide Al_2O_3 SPM 95		Tungsten (W) W_{25}		Tungsten oxide (WO_3) $D_{100\ oxidised}$	
Morphology	Angular		Spherical		Nanoparticles cluster	
$D_{psae\ 50\%}$[2] (µm, σ)	9.96 µm (5.37 µm)		7.56 µm (8.24 µm)		2.80 µm (3.34 µm)	
SEM image	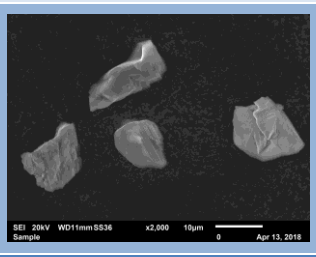		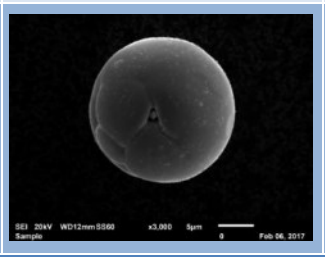		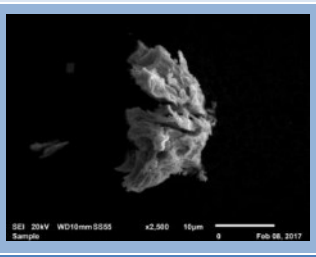	
Deposit characteristics						
Mass deposited (mg)	4.31	19.5	7.4	49.0	8.1	47.0
N_{mono}	0.09	0.41	0.30	2.04	0.05	0.27
Contact angle (°, k=2)	80.42 (2.45)	84.15 (4.28)	68.86 (1.05)	73.95 (2.55)	75.03 (2.02)	87.00 (5.61)

[2] $D_{psae\ 50\%}$ = median projected surface area equivalent diameter; diameter of a spherical particle with the same projected area as the particle in question and determined using a Malvern Morphologi G3 optical microscope with automatic analysis.